Heliyon 8 (2022) e09445

Contents lists available at ScienceDirect

Heliyon

journal homepage: www.cell.com/heliyon

Research article

On-chip testing of a carbon-based platform for electro-adsorption of glutamate

Y. Whulanza [a,b,*], Y.B. Arafat [a,c], S.F. Rahman [b,c], M.S. Utomo [d], S. Kassegne [e]

[a] Department of Mechanical Engineering, Faculty of Engineering, Universitas Indonesia, Indonesia
[b] Research Center on Biomedical Engineering, Universitas Indonesia, Indonesia
[c] Biomedical Engineering Program, Department of Electrical Engineering, Faculty of Engineering, Universitas Indonesia, Indonesia
[d] National Research and Innovation Agency, Tangerang Selatan, 15314, Indonesia
[e] Department of Department of Mechanical Engineering, College of Engineering, San Diego State University, San Diego, CA 92182, USA

ARTICLE INFO

Keywords:
Carbon matrix
Glutamate
Microfluidic system
Neurotoxicity
Neurotransmitter uptake and reverse uptake

ABSTRACT

It is known that excessive concentrations of glutamate in the brain can cause neurotoxicity. A common approach to neutralizing this phenomenon is the use of suppressant drugs. However, excessive dependence on suppressant drugs could potentially lead to adversarial side effects, such as drug addiction. Here, we propose an alternative approach to this problem by controlling excessive amounts of glutamate ions through carbon-based, neural implant–mediated uptake. In this study, we introduce a microfluidic system that enables us to emulate the uptake of glutamate into the carbon matrix. The uptake is controlled using electrical pulses to incorporate glutamate ions into the carbon matrix through electro-adsorption. The effect of electric potential on glutamate ion uptake to control the amount of glutamate released into the microfluidic system was observed. The glutamate concentration was measured using a Ultra Violet-Visible spectrophotometer. The current setup demonstrated that a low pulsatile electric potential (0.5–1.5 V) was able to effectively govern the uptake of glutamate ions. The stimulated carbon matrix was able to decrease glutamate concentration by up to 40%. Furthermore, our study shows that these "entrapped" glutamate molecules can be effectively released upon electrical stimulation, thereby reversing the carbon electrical charge through a process called reverse uptake. A release model was used to study the profile of glutamate release from the carbon matrix at a potential of 0–1.5 V. This study showed that a burst release of glutamate was evident at an applied voltage higher than 0.5 V. Ultimately, the MTS (3-(4,5-dimethylthiazol-2-yl)-5-(3-carboxymethoxyphenyl)-2-(4-sulfophenyl)-2H-tetrazolium) test for cytotoxicity indicated a cell viability of more than 80% for the carbon matrix. This test demonstrates that the carbon matrix can support the proliferation of cells and has a nontoxic composition; thus, it could be accepted as a candidate material for use as neural implants.

1. Introduction

L-Glutamate is an excitatory neurotransmitter with a major role in the mammalian central nervous system [1, 2, 3, 4]. A high concentration of L-glutamate in the extracellular fluid due to excessive release may play a major neurotoxic role in a wide range of neurological disorders [5, 6, 7, 8, 9, 10]. Thus, a system capable of controlling the release of L-glutamate might contribute to maintaining physiological and pathological states in the central nervous system [11, 12, 13, 14, 15].

In recent years, there has been growing interest in the realization of "intelligent" implants capable of controlling the release of therapeutic substances in response to external physical or chemical stimuli. Research on controlled drug release has made it possible to deliver various chemical substances at a constant rate and to a specific spatial target [16, 17, 18, 19]. A potential-controlled release and uptake system is attractive since it can provide precise control and an application of the stimulus electricity quickly, reversibly, and locally [20].

A molecular imprinting method was previously introduced for neurotransmitter uptake into an over-oxidized conducting polymer. However, this method requires pretreatment of polypyrrole, which includes oxidizing and exchanging ions [21, 22, 23]. Therefore, this study proposes an easier uptake method for a neurotransmitter using carbon-based materials. Additionally, the screen-printed, carbon-based material is more affordable than the conducting polymer. Several studies

* Corresponding author.
E-mail address: yudan.whulanza@ui.ac.id (Y. Whulanza).

https://doi.org/10.1016/j.heliyon.2022.e09445
Received 20 October 2021; Received in revised form 30 January 2022; Accepted 11 May 2022

Table 1. Screen-printing parameters.

Parameter	Value
Squeegee pressure	4 Kgf
Squeegee speed	5 mm/s
Print gap	0.5 mm
Mesh ruling	110 thread/cm
Thread diameter	45 μm
Mesh aperture size	54 μm

have also shown that carbon-based materials are effective in adsorbing active agents in antibiotics and aspirin [24, 25, 26, 27].

The ultimate goal of our work is to develop a neural implant (in-vivo) that is able to tune the neurotransmitter concentration. Achieving this goal would require characterizing the neural recording and stimulating capabilities of microelectrodes integrated into the system. Vomero et al. performed both in-vitro and in-vivo tests of neural recording using glassy carbon electrodes. They also confirmed the ability of electrodes to resist intense and prolonged current stimulation patterns by repetitively applying pulses with a current amplitude of 1 mA. Furthermore, the characterization of electrode using cyclic voltammetry of dopamine signals was completed using a range of 0.5–1.5 V applied potential [28].

At this moment, the tool presented in this study is meant to be a platform for understanding the release and uptake of L-glutamate neurotransmitters, so that a wider opportunity for the use of a microfluidic system to enable controlled L-glutamate release can be achieved. Based on the study outcomes, the basic premise of using a modified version of this system will be established in this paper to be applied in a future in-vivo neural implant [29, 30, 31, 32].

The focal point of this work is to develop neural interfaces in which glutamate concentration can be controlled by adsorbing glutamate into a screen-printed carbon matrix. Additionally, a reverse uptake study will be carried out to emulate the brain interface. Eventually, the uptake and monitoring system can be applied for the physiological modeling of neurons in an in-vitro microfluidic system, a topic that we have researched before [33, 34, 35].

2. Materials and methods

2.1. Preparation of carbon matrix

A conductive carbon paste from MJ Chemical (Jakarta, Indonesia) was mixed with multi-walled carbon nanotubes (MWCNTs) from Nanjing Xanano Materials Tech Ltd. (Nanjing, China). The carbon ink mixture mixed under ultrasonic vibration for 10 min was ready to be used as a carbon electrode, as detailed below. The MWCNT content in the mixture had a concentration of 5% w/w. A flame-retardant substrate normally used as a printed circuit board (PCB) was utilized in this study. A silk screen was placed onto the substrate, and a drop of carbon paste was layered onto the stencil. A squeegee was pushed in a single-direction movement to apply the carbon paste throughout the screen printing. The PCB was then heated on a hotplate at 120 °C for 5 min. A second deposition was repeated in the exact same manner to realize the 3D texture of the matrix [36]. Table 1 shows the screen-printing parameters.

2.2. Characterization of the carbon matrix

Electrical performance was characterized using a four-probe tester, RTS-8, from Four Probes Technology (Guangzhou, China), and measured using a 4-point sheet resistance with 2 mm electrode spacing. The thickness of the carbon matrix was measured using an Elcometer 456 induction gauge (Manchester, UK), which was zeroed on the substrate base. Four repetitive measurements were taken for each of the five substrates.

The surface morphology of the carbon matrix was observed using a scanning electron microscope (SEM) instrument from Phenom ProX-G6 Thermofisher Scientific (Waltham, US). A back scattered detector (BSD) was used to obtain a magnification of 500–2000 times. Component identification was performed using the energy dispersive spectrometer (EDS) mode.

The adhesion of the carbon matrix to the PCB substrate was determined using the adhesive tape test (ASTM D 3350–02) [37]. First, a carbon matrix specimen, 2 mm wide and 5 mm long, was prepared exactly as the screen-printing preparation mentioned above. The carbon matrix was cut using a razor to form a cross-hatch. An adhesive tape (Elcometer 99, Manchester, UK) was applied firmly to cover the sample area. Later, the adhesive tape was stripped off with one quick peeling. The quality of the screen-printed carbon matrix can be assessed by comparing the number of squares peeled off to the total number of squares.

2.3. Microfluidic chip fabrication

At the beginning of the process, a chip mold was designed in the Autodesk Inventor 2019 CAD program (San Rafael, USA). Overall, the chip was 7.5 cm long, 2.5 cm wide, and 0.6 cm thick. The chip contained two layers: a bottom layer and a top layer, as shown in Figure 1b. The microfluidic chip consisted of several sections: an inlet point, an uptake chamber, a flow valve (passive), and a sampling point (Figure 1b). The microfluidic chip also had two main layers: the top layer, which confined the glutamate solution, and the bottom layer, which was embedded with a flame retardant (PCB) substrate. A 1-mm-wide microchannel connected the inlet, uptake chamber, and detection chamber in the top layer. The PCB portion used the carbon matrix substrate as the base of the uptake chamber lid. The metal lid was platinum-coated titanium, available in the

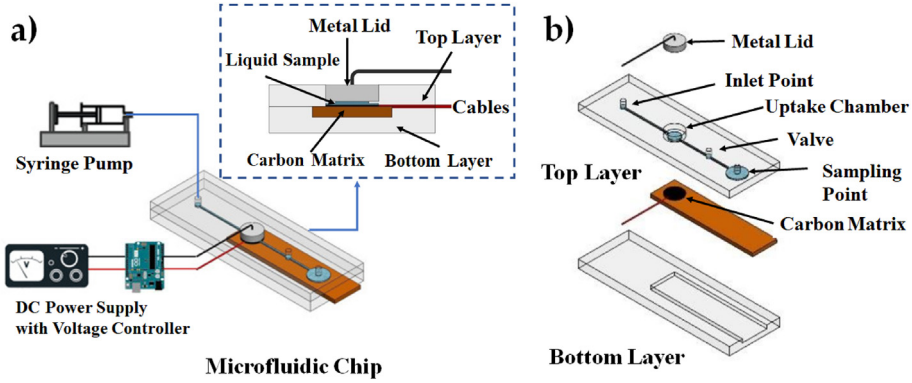

Figure 1. (a) Schematic diagram of a microfluidic chip in a release study platform; (b) breakdown of the microfluidic chip integrating the uptake chamber with a carbon matrix underneath and a metal lid on top.

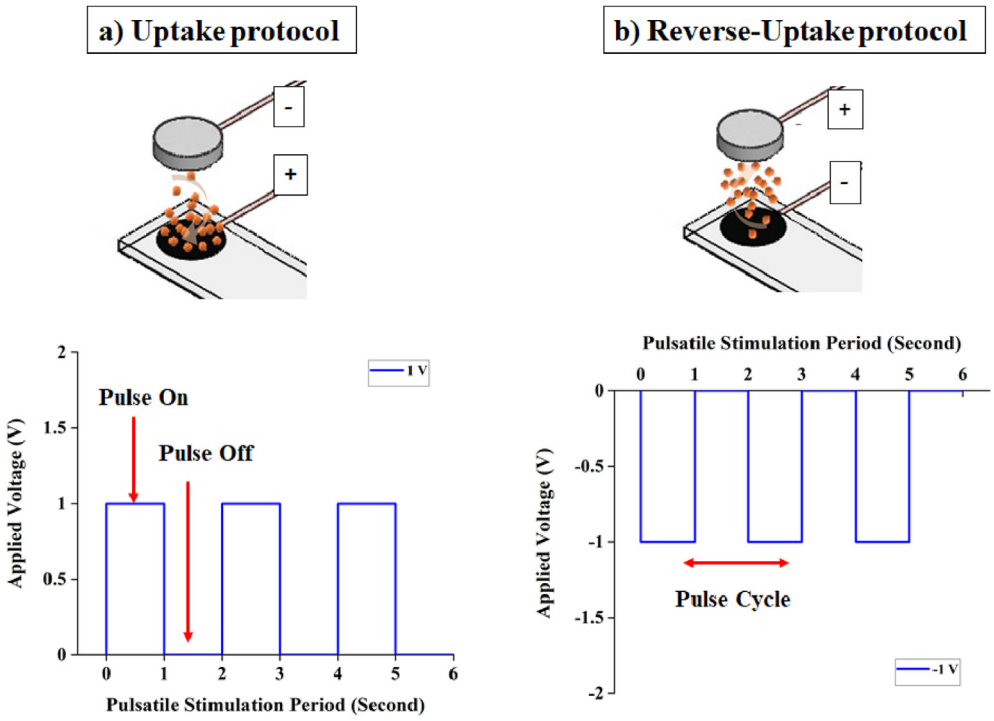

Figure 2. Pulsatile stimulation of the carbon matrix during both protocols: a) uptake and b) reverse uptake of glutamate ions in the solution. The pulsatile stimulation forms 50% of the duty cycle.

form of round bars 8 mm in diameter from Polymet-Reine Metalle (Lunenburg, Germany). The round bar was originally supplied at a length of 100 mm, which was then cut into 2.5 mm sections using a wire-cut electric discharge machine (Fanuc Robocut Alpha C400iA, Oshino-mura, Japan).

An EMCO VMC 200 (Hallein, Austria) milling machine was used with an accuracy of 1/100 mm to fabricate the chip mold. Polydimethyl siloxane (PDMS) Sylgard 184 from Dow Corning (Midland, USA) was cast in an aluminum mold. The PDMS was mixed beforehand with its curing agent at a ratio of 10 to 1. The mold was placed inside a vacuum chamber to eliminate air bubbles trapped in the PDMS during the mixing process. Afterwards, the mold was heated in a hot chamber for 15 min at 140 °C and then peeled. Similar steps were carried out to fabricate the bottom part.

Figure 1 shows a complete set of microfluidic chips that include a carbon electrode that is readily prepared on the PCB substrate. The electrode was then sandwiched between the PDMS top and bottom layers. The PDMS top and bottom layers were bonded using a Corona SB plasma treater from BlackHole Lab (Paris, France) for 30 s on each surface of the layer. The step-by-step arrangement of the chip is depicted in Supplementary Figure 1.

The sterilization of the microfluidic chip was performed using an SUN series autoclave using the Ningbo Mingtai Medical Instrument (Ningbo, China). All microfluidic chips were placed into autoclave pouches and sealed prior to the sterilization step. The autoclave chamber was arranged to be exposed to saturated steam at a temperature of 121 °C and a pressure of 115 kPa for 20 min.

2.4. Setup of the microfluidic system

Figure 1a shows a schematic diagram of a microfluidic chip to be utilized in a microfluidic system to emulate a neural implant. A syringe pump (NE-1000 New Era, Farmingdale, USA) was used to insert the glutamate solution into a microfluidic chip that integrated the uptake process. The uptake chamber was filled with around 100 μL of glutamate solution in each uptake and reverse uptake protocol. The uptake chamber was designed to have a carbon matrix at the base and metal as the lid. The glutamate uptake protocol was carried out by applying voltage to the carbon matrix using a DC power supply. An open-source microcontroller board from Arduino Srl (Genova, Italy) was used to generate the desired electric potential. This charged matrix attracted glutamate anions in the liquid specimen. Once the uptake process was completed, the liquid specimen was allowed to flow through the sampling point chamber by manually opening the valve (Microfluidic-ChipShop, Jena, Germany). A liquid sample of 100 μL was taken out of the detection chamber using a UV-visible spectrophotometer.

2.5. Preparation of the glutamate solution

The glutamate solution was prepared by dissolving L-Glutamic acid (Sigma Aldrich, Darmstaadt, Germany) in deionized water. A mother liquor of glutamate solution was prepared using 0.1 mg/mL to be equal to 0.68 mM glutamate in water. Various concentrations of glutamate were prepared by diluting the mother liquor into five concentrations: 34, 68, 102, 136, and 170 μM. These concentrations were prepared as a standard curve for detection. We used deionized water as the baseline curve, which was subtracted from the readings of the above concentrations. The selection of concentrations was aligned with the physiological glutamate release in the body at around 20–100 μM.

2.6. Preparation of pre-adsorbed glutamate on the carbon matrix

A carbon matrix adsorbed with glutamate ions was prepared by confining the glutamate mother liquor (0.1 mg/ml) in the uptake chamber, which was electrostimulated for 1 min. The chip was then kept in the fume hood for another 6 h for drying. It was assumed that adsorption would take place during this immersion period. Later, the microfluidic chamber was flushed gently by circulating deionized water for three cycles using a syringe pump at a rate of 20 μL/h.

2.7. Study of electrostimulation uptake and reverse uptake

The assembled chip was filled with a concentration of glutamate solution until the uptake chamber was filled to around 100 μL. Electrical stimulation was generated and controlled by a digital direct current power supply (GW Instek, Taipei, Taiwan). A carbon matrix electric pad was connected to a positive pole, while the metal lid served as a negative electrode (Figure 2). A square wave potential was applied to aid in the uptake of glutamate ions from the glutamate solution into the carbon matrix. Figure 2a shows a pulsatile stimulation with a duty cycle of 50%. Each pulse cycle had a period of two minutes and was repeated for 10 cycles, with applied voltages of 0.5, 1, and 1.5 V. A protocol with a non-stimulated potential of 0 V was also performed for comparison with the stimulated protocols. In this uptake protocol, a glutamate solution with a concentration of around 100 μM was used.

The reverse uptake protocol was carried out by switching the poles so that the carbon matrix would be negatively charged, while the metal lid would be positively charged (Figure 2b). In the case of reverse uptake, deionized water was used as the liquid media in the chamber with a pre-adsorbed glutamate carbon matrix. The stimulation protocol was applied in a manner similar to the uptake process, as depicted in Figure 2b.

The uptake and reverse uptake processes were validated by measuring the glutamate concentration in the liquid specimen sample from the microfluidic chip using a UV-visible spectrophotometer from Shimadzu (Kyoto, Japan). Sampling was performed after each pulse cycle, and a new chip was prepared for the next setup of the pulse cycle. Four sample replications were used in each measurement group.

2.8. Measurement of glutamate concentration using a uv-visible spectrophotometer

The glutamate concentration in the liquid specimen was measured using a UV-visible spectrophotometer absorbance (Shimadzu 3101PC, Kyoto, Japan) at a maximum wavenumber of 210 nm. A 100 μL sample was taken from the chip and placed in a quartz cuvette of the spectrophotometer. A calibration curve of glutamate was prepared by measuring the absorbance of various glutamate concentrations in the range of 30–180 μm. In addition, the standard curve of absorbance measurements for various concentrations was fitted using line oar regression. The limit of detection (LOD) was calculated as follows:

$$LOD = 3.3*SE/S \quad (1)$$

Where SE and S are the standard error and slope of the calibration curve, respectively.

2.9. Cytotoxicity assay

Three groups of samples were prepared: a polymer multiwell base, a flame retardant (PCB support) carbon matrix on a flame-retardant substrate, and a pre-adsorbed glutamate carbon matrix (glu-carbon). IMR-32 neuroblast cells from ATCC (Manassas, VA, USA) were then seeded on a multiwell plate at around 250,000 cells/cm^2 and incubated in Dulbecco's Modified Eagle Medium (Lonza, Basel, Switzerland), with 200 mM of 1% L-Glutamine (Lonza, Basel, Switzerland), 10% FBS (Lonza, Basel, Switzerland), 1% penicillin/streptomycin/amphotericin B ((Lonza, Basel, Switzerland)), 1% MEM vitamin solution, (Sigma Aldrich, Darmstaadt, Germany), and 1% non-essential amino acids 100X (Sigma Aldrich, Darmstaadt, Germany), along with the three sample groups. A CellTiter-Blue assay (Promega, Madison, WI, USA) was also performed on all samples. Cell viability measurements were carried out at 24, 48, and 96 h after seeding. The control measurement of the multiwell base seeded with the cells was performed 24 h after seeding. The viability of the other substrates was normalized to the viability of the control. Three repetitive samples were applied for each group's treatment.

Table 2. Properties of the carbon matrix.

Description	Resistivity (kΩ.m)	Thickness (um)	Note
Carbon ink	113.33 ± 7.2	6.4	Without CNT
Carbon matrix	0.36 ± 0.1	28.2 ± 1	CNT blended
Glu-carbon	0.48 ± 0.2	28.2 ± 1	Glutamate adsorbed

2.10. Statistical analysis

All glutamate concentration measurements are presented as mean ± standard deviation. Two factors that affected the magnitude of glutamate uptake concentration were applied potential and pulse cycles. A two-way ANOVA was used to test the significance of the variables and to observe the correlation of the measured glutamate concentration in the liquid sample with the applied voltage and the pulse cycle. Statistical analyses and curve fitting were performed using Origin software version 2020b (Northampton, US).

Similarly, a statistical test was conducted to analyze the results of the biocompatibility test for different substrates during various cell seeding times. All results were assumed to follow a normal distribution. A significance level of 0.05, which will be compared to the calculated statistical P-value, was used in this study.

3. Results and discussion

3.1. Material characterization of the carbon matrix

The thickness of the carbon matrix was measured using an induction gauge instrument that compared the distances before and after the screen-printing process on the flame-retardant support. The thickness of the screen-printed carbon paste before it was blended with the carbon nanotubes was also observed; these values are summarized in Table 2. The measurements showed that the carbon matrix had a thicker layer compared to the carbon paste without the CNT blend. Table 2 also shows that the thickness of the adsorbed glutamate carbon matrix was not significantly different from that of the carbon matrix.

The resistivity of these specimens was also measured and is listed in Table 2. The surface resistivity of the carbon layer without the CNT blend was around 110 kΩ.m. The blending of the carbon matrix with CNT significantly decreased the resistivity to around 0.4 kΩ.m. These results are similar to those found by Du et al. and Menon et al., who worked on improving electrodes using the screen-printing method [38, 39]. The measurements of resistivity for the carbon matrix and the pre-adsorbed carbon matrix were, on average, 0.36 ± 0.1 kOhm.m and 0.48 ± 0.2 kOhm.m, respectively. These statistics indicate that the deviation of the samples was relatively high; however, the samples were not significantly different. Note that a maximum of 100 μg of glutamate was added to the carbon matrix utilized in this setting.

The quality of the screen-printed carbon matrix was determined using the peel test method. Figure 3 shows the results of the peel-off test. This method helps determine the quality of the carbon matrix on the PCB substrate. The peeling test was also carried out to distinguish the carbon matrix before and after glutamate adsorption. Figure 3a shows the carbon substrate without a glutamate coating on the PCB matrix, which was then cut using a razor, as shown in Figure 3b. Subsequently, adhesive tape was applied and lifted off, which resulted in the image shown in Figure 3c. Similarly, the carbon matrix with glutamate adsorption is depicted in Figures 3d–3f. A visual comparison of Figures 3c and 3f indicates that there is no significant difference in the quality of the carbon coating before and after glutamate pre-adsorption.

Magnified images of the carbon matrix before and after the pre-adsorption process are shown in Figure 4. Figure 4a depicts the “plain” carbon matrix before going through the glutamate pre-adsorption process. An inset figure is also included to show the carbon electrode. Figure 4b shows the carbon matrix after the pre-adsorption process.

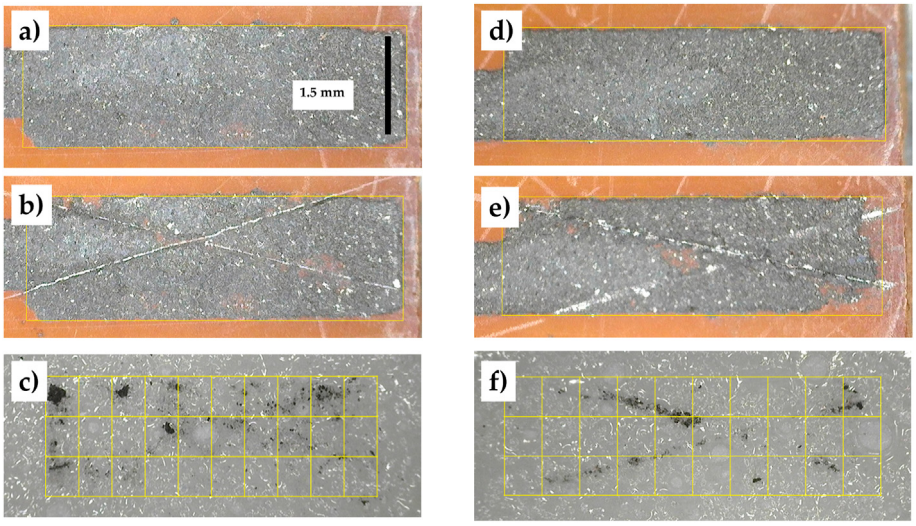

Figure 3. Peel-off result of the screen-printed carbon matrix based on the adhesive tape test conducted on two specimens: a-c) before and d-f) after the pre-adsorption of glutamate.

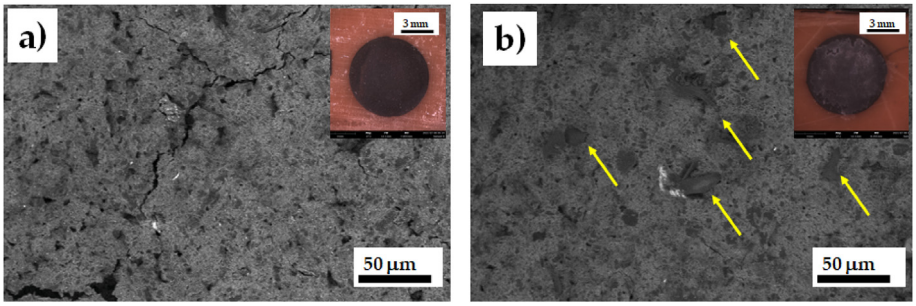

Figure 4. Observation of the carbon matrix: (a) before and (b) after the glutamate pre-adsorption step using a scanning electron microscope, with a photograph of the carbon electrode in the inset.

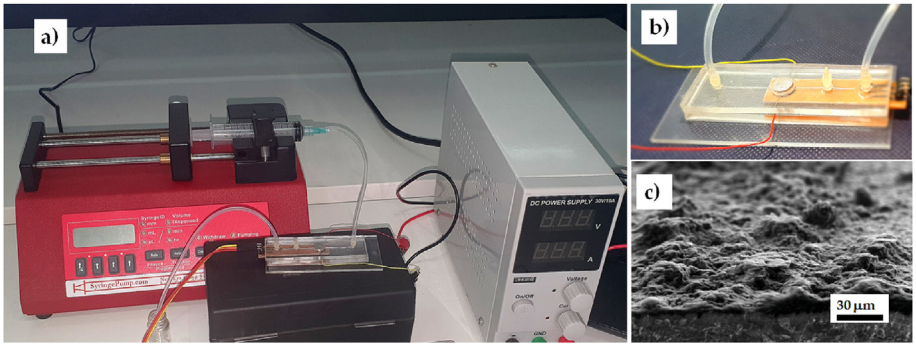

Figure 5. The setup of the microfluidic system, realized by emulating the glutamate uptake and integrated with detection: (a) the setup consisting of a syringe pump, microfluidic chip, and power supply; (b) the assembled microfluidic chip equipped with a connection pad to an electrostimulation power supply; and (c) the microstructure of the carbon matrix that resulted from the screen-printing method.

Overall, glutamate entities were not visible in the carbon matrix, unless in its crystal form, as indicated by yellow markers.

These crystals formed during the evaporation of the glutamate solution during the pre-adsorption process. The initial concentration of glutamate liquid was 0.1 mg/ml, whereas the solubility limit is known to be around 8.5 mg/ml. Therefore, some portion of glutamate is adsorbed into the solid body until its saturation concentration. The remaining glutamate will be suspended as crystals and entrapped in the carbon matrix, as shown in Figure 4b.

3.2. Microfluidic system setup

The complete setup of the microfluidic system is depicted in Figure 5a. The glutamate solution was delivered into the microfluidic chip with a syringe pump at a rate of 2 mL/h. The PCB inserted into the microfluidic chip served well as the base of the uptake chamber and the detection chamber (Figure 5b). The carbon matrix, depicted in the inset in Figure 5c, was then magnified to observe the surface of the carbon matrix.

3.3. Measurement of glutamate concentration

The UV-Vis spectra were recorded for solutions with concentrations of 34, 68, 113, and 136 μM on a standard curve. This research only considered a physiologically relevant concentration of glutamate in the range of 20–100 μM; therefore, a higher glutamate concentration was not required. As seen in Figure 6, there was a large peak at 190 nm and a shoulder at 200 nm. These values indicate strong absorption in the 190–220 nm range.

Here, a standard curve of the UV absorbance–glutamate concentration was determined for a reading of around 210 nm. The linear correlation depicted in Figure 6 is as follows: Absorbance (Absorbance unit) = 0.0088*Concentration Glutamate (μM) + 1.1209. The quality of fit coefficient (R^2) was 0.981. The linear detection of the glutamate solution using this method was estimated to be around 27 μM (calculated using Equation 1).

3.4. Passive release study

A passive release study was carried out to observe glutamate release from the pre-adsorbed carbon matrix. An additional observation was performed to confirm the amount of passive glutamate release. The observed adsorption phenomena adhere to Langmuir adsorption, where the molar concentration of the solution determines the equilibrium of the adsorbed ions by partial pressure. Significant low resistivity was observed when a solution with 0.1 mg/mL of glutamate concentration effectively shifted the equilibrium towards higher anion adsorption on the surface. A higher glutamate concentration would lower the resistivity while limiting glutamate solubility in water. Glutamate releases higher than the physiologically relevant concentration range (20–80 μM) was not observed in the current setting.

The glutamate release profiles from the carbon matrix with various concentrations of initial glutamate seeding are also presented in Figure 7. In the current setting, the study was conducted over a duration of 28 days. As predicted, a higher glutamate concentration during initial seeding would lead to a higher glutamate release. In other words, the amount of glutamate ions electrostatically trapped inside the carbon matrix corresponds to the glutamate concentration during initial seeding.

It is assumed that glutamate release will show a profile similar to an active agent in drug release studies [16, 17, 22]. The proposed model is a

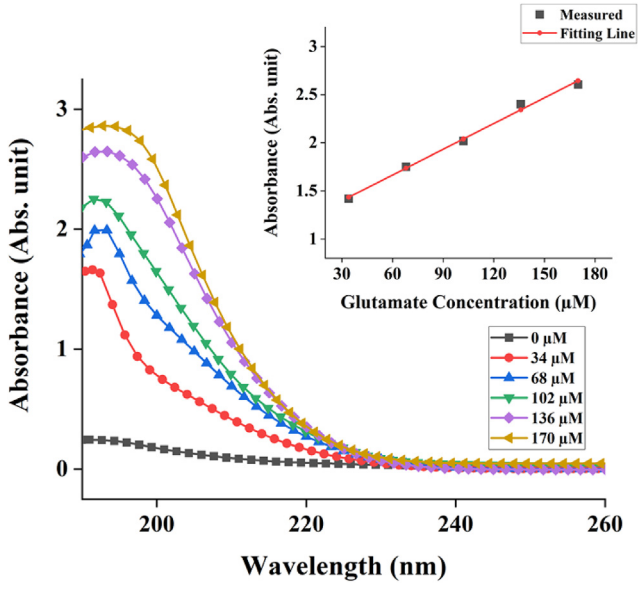

Figure 6. Measurement of glutamate concentration using the UV-Vis method, with an inset graph of the standard curve of glutamate concentrations for 0–113 μm glutamate.

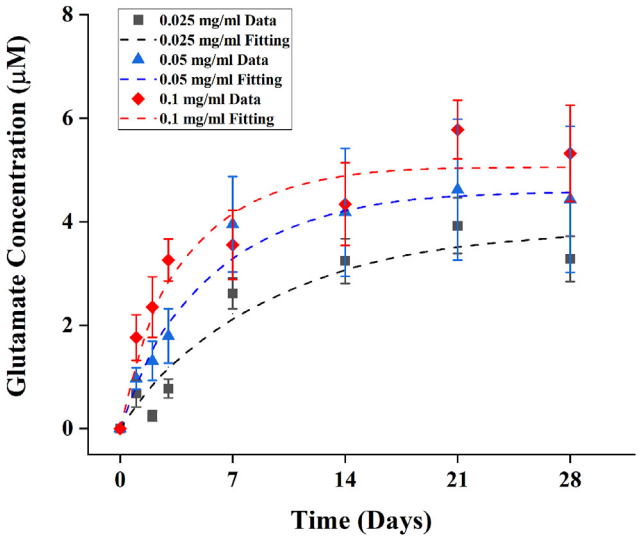

Figure 7. Profile of glutamate concentration in the liquid sample in the passive release mode, which is equivalent to the unstimulated mode in the reverse uptake setup, for 28 days of observation.

non-linear first-order exponential equation. The glutamate concentrations during the passive studies were fitted using the exponential growth equation, as follows:

$$y = a\,(1 - e^{(-bx)}) \quad (2)$$

Where x is the time and a and b are constants. 'y = a' is the asymptotic model equation. This asymptotic equation can be interpreted as follows: When the stimulation is close to infinity, the glutamate concentration tends to reach a constant. The reciprocal parameter 'b' or 1/b indicates the time (in days) needed to achieve that constant concentration. It is noted that the b parameter corresponds to the glutamate release profile.

Figure 7 shows an increasing concentration of glutamate in the liquid sample, from around 2 μM on day 1 to a saturation point of around 5 μM on day 21. We observed a passive release profile, which was then fitted using an exponential growth model, as shown in Eq. (2). The model parameters are summarized in Table 3. The fitting results showed an R correlation-based goodness of fit of 0.96. The model predicted a value close to the real data. Although a release of glutamate from the matrix was evident during the 28 days of observation, it can be assumed that the actual glutamate secretion is lower than what was observed in the current study. The over accumulation of glutamate can be omitted since it would be removed from the circulatory system, considering the brain to be a continuously circulated system [40, 41, 42, 43].

3.5. Uptake and reverse uptake of glutamate

Monitoring the concentration of biomolecules in a fluid is one way to study the uptake and reverse uptake of biomolecules at the solid–liquid interface. Initially, around 100 μM of glutamate solution was channeled in the microfluidic chip and placed in the uptake chamber. The uptake process was then carried out by activating the DC potential supply to

Table 3. Parameters of the mathematical model.

Glu initial seeding (mg/ml)	a	b	Time Constant (1/b)	Quality of Fit R^2
0.025	3.829	0.124	8.065	0.939
0.050	4.581	0.204	4.901	0.982
0.100	5.056	0.291	3.436	0.919

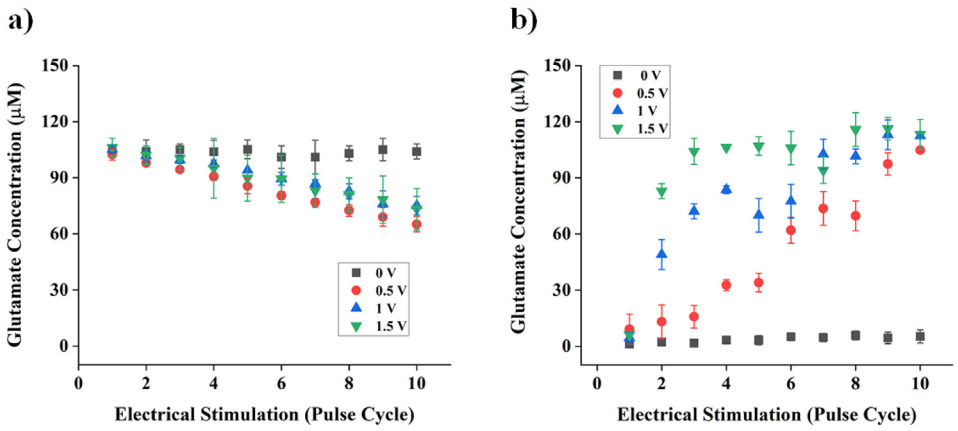

Figure 8. The measurement of glutamate concentration for various applied voltages: (a) the process of glutamate uptake into the carbon matrix; (b) reverse uptake of glutamate from the adsorbed glutamate carbon matrix.

determine the duration of the uptake. Once the uptake process was completed, the glutamate concentration in the liquid was measured using a spectrophotometer. Our study measured glutamate concentration in the liquid, which was affected by the applied potential and the number of pulse cycles. It is essential that the concentration of extracellular glutamate is kept low. The excessive activation of glutamate receptors is dangerous, and in high concentrations, glutamate is toxic [11]. The platform demonstrates glutamate uptake and the reverse uptake mechanism. The benefit will be the direct regulation of neurotransmitter uptake and release and special access to successive neurons.

A voltage of around 1 V was utilized in this step, based on a study by Paul in which a stimulation of 0–1 V was utilized. The report also suggested using this potential in the future application of the implant in the human body for safety reasons. The previous works of Nimbalkar et al. and Vomero et al. showed the viability of cells on the glassy carbon substrate using stimulations of 0.5–1.5 V. The applied potential was limited to a maximum of 1.5 V to avoid the water electrolysis phenomenon. Ma et al. conducted an electro-adsorption study that utilized a potential of 1–1.5 V to the solution, in which no electrolysis occurred. Additionally, Givirovksy et al. reported that the water electrolysis phenomenon was evident in their small-scale electro bioreactor at an applied potential of 2 V.

Studies have shown that brain electrical stimulation for clinical therapy utilizes pulses with 0.1–1 s of pulse time [44]. Additionally, a maximum exposure of electrical stimulation with a few cycles (<15 cycles) was the established general practice. The clinical treatment aimed to obtain a balanced state of neurotransmitters in the brain [44, 45]. Therefore, there would be interactions between the evoked stimulation and the neuron responses, which occur within a short amount of time. In this case, it can be concluded that pulsatile stimulation is more appropriate, considering that the neuron responses due to the stimulation were expected to be observed.

Figure 8a indicates that the applied potential has a considerable effect on the glutamate solution in the chip during the uptake process. Figure 8a shows that glutamate concentration has a decreasing trend along with the stimulation cycle. Notably, the decreasing concentration was initiated during the second pulse cycle. It was presumed that the glutamate anions' uptake and adsorption was not observable in the first pulse cycle. The uptake of glutamate anions was accomplished by adsorbing the anions into the charged carbon matrix. The glutamate anions were repulsed from the metal lid and attracted by the opposite charge of the carbon matrix. On the contrary, the non-stimulated mode, 0 V, demonstrated that the glutamate concentration remained at around 103 μM during the observation time.

As shown in Figure 8a, the concentration of the glutamate liquid sample ranged from 100 to 60 μM. Note that the initial glutamate concentration was around 100 μM. The glutamate uptake was apparent, indicated by the decreasing concentration around 40 μm for all the applied stimulations at the end of the cycles.

Here, the applied potential and pulse cycle were the two variables considered to affect the glutamate uptake concentration in the liquid sample. Therefore, a two-way ANOVA calculation with Bonferroni correction was employed and returned a p-value of 0.649 for the interaction of applied voltage and pulse cycle. These values suggest that the glutamate concentration in the liquid sample resulted in a similar outcome for all stimulation voltages.

To further characterize the interaction of the carbon matrix and glutamate solution in the microfluidic system, a reverse uptake study was carried out. Here, reverse uptake was carried out by reversing the charge of the power supply. The metal lid acted as a positive pole and the carbon matrix was negatively charged. Thus, the glutamate anions were repulsed by the carbon matrix and released into the liquid body. In this experimental setup, a pre-adsorbed glutamate carbon matrix was utilized in the chamber. Moreover, deionized water was used to indicate a zero concentration of glutamate in the initial reverse uptake study.

Figure 8b shows the reverse uptake stimulation using a similar potential in the uptake study. The non-stimulated mode, 0 V, resulted in a glutamate concentration of around 5 μM after the final pulse cycle. This value is similar to the initial glutamate concentration in liquid. It was found that all applied stimulations resulted in a similar final concentration after the 10 cycles, which was around 100–110 μM. However, the release profile for the glutamate concentration varied between the applied voltages. Although the terminal concentration was similar, the 0.5 V stimulation showed a linear profile, whereas the 1 and 1.5 V stimulations demonstrated a burst release profile (Figure 8b). This initial burst allows the release of a relatively large quantity of neurotransmitters in the first 2–3 min and then few neurotransmitter (if any) are released further. This burst concentration was evident in the second pulse cycle.

A statistical calculation was made to confirm this finding. A two-way ANOVA calculation with Bonferroni correction was employed and returned a p-value of less than 0.05 for the interaction of applied voltage and the number of pulse cycles. This value suggests that glutamate concentration is significantly affected by both the parameters applied and the number of pulses.

The 0.5 V voltage provides the most favorable applied voltage for two reasons: first, it is safe in the human body, and second, it provides optimum uptake and reverse uptake settings. Our uptake result shows that a non-significant difference results were shown for the applied voltages from 0.5–1.5 V. Moreover, the reverse uptake protocol showed a linear profile at the 0.5 V applied voltages. This so-called time lag reduces the burst release characteristic, which is undesirable in controlled release systems.

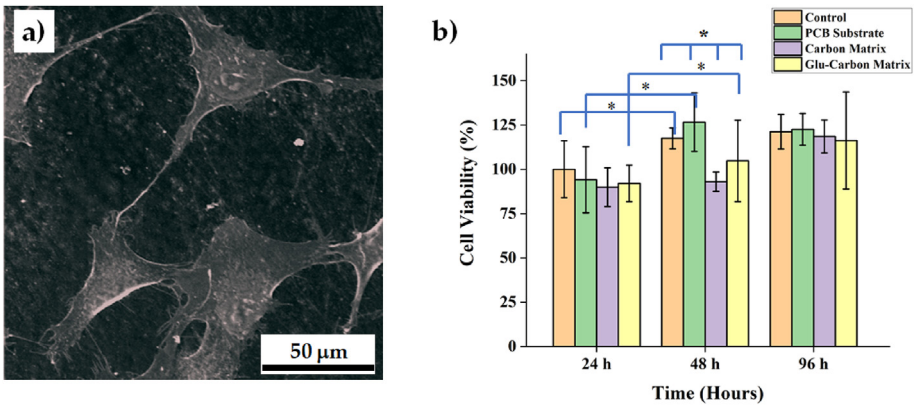

Figure 9. (a) The result of electron microscope observation for the cortical neuron cells on the carbon matrix substrate and (b) the measurement of cell viability using the MTS method at various layers: PCB substrate, carbon matrix, and carbon matrix adsorbed by glutamate. An asterisk indicates a statistically significant difference between the two groups.

3.6. Electroadsorption mechanism

The mechanism of uptake is similar to the findings of Paul et al. [21]. They studied uptake and reverse uptake processes using a molecularly imprinted polymer (MIP) and found a relationship between glutamate concentration and voltage pulse on the MIP electrode. They found that positive voltage decreased the glutamate concentration, while negative voltage increased the glutamate concentration. Since glutamate has a negative charge, the positive voltage attracts glutamate. The glutamate concentration decreases for voltage between 0.5–1.5 V, which can be interpreted as binding glutamate ions to the positively charged carbon electrode of the negatively charged glutamate molecules, leading to a reduction in the number of glutamate molecules in the solution. Since a charged carbon matrix was employed as a positive electrode, the reduction in glutamate concentration in the liquid sample was possibly due to the adsorption of glutamate into the carbon surface [25].

Deore et al. found that the L-glutamate adsorption quantity increased dramatically with a decreased potential from +0.6 to 0 V, whereas it decreased again when the potential shifted from −0.1 to −0.3 V [23]. Depending on the pH, the chemical structure of glutamate varies from acidic (NH_2RCOOH) to anionic (NH_2RCOO^-), to cationic (NH_3^+ RCOOH), or to zwitterionic (NH_3^+ $RCOO^-$) [46]. Glutamate in the zwitterionic form, which is the most essential for biological processes, occurs in the pH range of 4.3–9.7 [21]. Glutamate has a net negative charge, two of which are negatively charged by deprotonated carboxylates and one by the protonated amine group [23]. This charge was utilized to uptake and reverse uptake glutamate anions using a charging surface carbon electrode.

3.7. Biocompatibility

The normal reaction when inserting the cell tissue into the substrate is the production of a fibrous capsule [47]. By forming a barrier between it and the surface, this fibrous structure can obstruct the measurement of neurotransmitters with the implants and has been suggested as the key explanation for in vivo implant failure [48]. Here, we performed an MTS assay using human neuronal cells to study the proliferation of the cell through cell viability. Based on the morphological visualization in Figure 9a, the carbon matrix surface exhibited great biocompatibility. The shape of the cell attached to the surface of the carbon matrix and adapted to start proliferating. It was also observed that the cell spread in the carbon matrix equally to the control substrate (Supplementary Figure 2).

The results of the MTS assay on various substrates are shown in Figure 9b. Here, the polystyrene multiwell was used as the control value. The assay demonstrated that the cell viability on PCB, carbon, and glutamate-carbon substrates was comparable to the control (cell on a multiwell base). The percentage of surviving cells increased progressively after 2 days for most substrates and remained constant afterward. This fact was supported by the statistically significant difference in results from 24 to 48 h of seeding time (indicated by the asterisk in Figure 9b). The MTS result also showed that the cell seeding on the PCB substrate resulted in a similar viability to the control in every cell seeding time. Additionally, Figure 9b demonstrated that there is no significant difference among all different substrates, specifically at 24 h and 96 h of cell seeding. The carbon matrix substrate showed the lowest proliferation during this period, although it reached a similar viability with other substrates in 96 h of observation. This finding is in accordance with an existing study that indicates carbon-based materials have been proven to be biocompatible for the growth and differentiation of various cells, including neurons, osteoblasts, and stem cells [48, 49, 50, 51, 52, 53, 54].

4. Conclusions

A microfluidic system has been successfully built as a platform to study the uptake and reverse uptake of glutamate. At this moment, we are in the initial phase of realizing our "neuron-on-chip" platform to emulate neuron activity and the interaction of neurons with our substrate. The results demonstrate that glutamate ions can be absorbed into a carbon matrix using an electrically driven conductive carbon layer. It was hypothesized that glutamate adsorption would be based on the duration and number of pulse cycles. It was found that the 0.5 V electric potential for both the uptake and reverse uptake processes showed a specific profile. This resulted in an adsorption of glutamate around 4–5 µM at each cycle. This amount is equal to 4–5% of the initial concentration of glutamate solution at each cycle. This voltage also suggests a linear reverse uptake (release) of glutamate from the substrate to the liquid. Ultimately, the biocompatibility of the carbon matrix electrode was studied using an MTS assay with human neuronal cells. According to morphological visualization and cell viability, the carbon matrix exhibits great biocompatibility. Therefore, it can be concluded that the current findings can be further applied to the development of modeling studies on neuronal pathological studies.

Declarations

Author contribution statement

Yudan Whulanza: Performed the experiments; Analyzed and interpreted the data; Contributed reagents, materials, analysis tools or data; Wrote the paper.

Yunus Bakhtiar Arafat: Conceived and designed the experiments; Performed the experiments.

Siti Fauziah Rahman and Muhammad Satrio Utomo: Analyzed and interpreted the data; Wrote the paper.

Samuel Kassegne: Conceived and designed the experiments.

Funding statement

This work was supported by Universitas Indonesia (KI NKB-795/UN2.RST/HKP.05.00/2020).

Data availability statement

Data included in article/supplementary material/referenced in article.

Declaration of interests statement

The authors declare no conflict of interest.

Additional information

Supplementary content related to this article has been published online at https://doi.org/10.1016/j.heliyon.2022.e09445.

Acknowledgements

The authors wish to thank Mr. David Tanny and Ms. Rani Panggabean from Dynatech International Ja-karta, for the Scanning Electron Microscope (SEM) observation support.

References

[1] B.S. Meldrum, Glutamate as a neurotransmitter in the brain: review of physiology and pathology, J. Nutr. 130 (4) (2000) 1007S–1015S.
[2] N. Talma, W.F. Kok, C.F. de Veij Mestdagh, N.C. Shanbhag, H.R. Bouma, R.H. Henning, Neuroprotective hypothermia–Why keep your head cool during ischemia and reperfusion, Biochim. Biophys. Acta Gen. Subj. 1860 (11) (2016) 2521–2528.
[3] L. Zhang, X.J. Kong, Z.Q. Wang, F.S. Xu, Y.T. Zhu, A study on neuroprotective effects of curcumin on the diabetic rat brain, J. Nutr. Health Aging 20 (8) (2016) 835–840.
[4] W.E. Bjorn-Yoshimoto, S.M. Underhill, The importance of the excitatory amino acid transporter 3 (EAAT3), Neurochem. Int. 98 (2016) 4–18.
[5] A. Mehta, M. Prabhakar, P. Kumar, R. Deshmukh, P.L. Sharma, Excitotoxicity: bridge to various triggers in neurodegenerative disorders, Eur. J. Pharmacol. 698 (2013) 6–18.
[6] M.D. Scofield, P.W. Kalivas, Astrocytic dysfunction and addiction: consequences of impaired glutamate homeostasis, Neuroscientist 20 (6) (2014) 610–622.
[7] J. Lewerenz, P. Maher, Chronic glutamate toxicity in neurodegenerative diseases—what is the evidence? Front. Neurosci. 9 (2015) 469.
[8] U. Vazana, R. Veksler, G.S. Pell, O. Prager, M. Fassler, Y. Chassidim, Y. Roth, H. Shahar, A. Zangen, R. Raccah, E. Onesti, M. Ceccanti, C. Colonnese, A. Santoro, M. Salvati, A. D'Elia, V. Nucciarelli, M. Inghilleri, A. Friedman, Glutamate-mediated blood–brain barrier opening: implications for neuroprotection and drug delivery, J. Neurosci. 36 (29) (2016) 7727–7739.
[9] J. Albrecht, M. Zielińska, Mechanisms of excessive extracellular glutamate accumulation in temporal lobe epilepsy, Neurochem. Res. 42 (6) (2017) 1724–1734.
[10] R. Wang, P.H. Reddy, Role of glutamate and NMDA receptors in Alzheimer's disease, J. Alzheim. Dis. 57 (4) (2017) 1041–1048.
[11] N.C. Danbolt, Glutamate uptake, Prog. Neurobiol. 65 (1) (2021) 1–105.
[12] G.W. Davis, M. Müller, Homeostatic control of presynaptic neurotransmitter release, Annu. Rev. Physiol. 77 (2015) 251–270.
[13] C. Murphy-Royal, J. Dupuis, L. Groc, S.H. Oliet, Astroglial glutamate transporters in the brain: regulating neurotransmitter homeostasis and synaptic transmission, J. Neurosci. Res. 95 (11) (2017) 2140–2151.
[14] Y. Kang, I. Hwang, Glutamate uptake is important for osmoregulation and survival in the rice pathogen *Burkholderia glumae*, PLoS One 13 (1) (2018).
[15] S. Mahmoud, M. Gharagozloo, C. Simard, D. Gris, Astrocytes maintain glutamate homeostasis in the CNS by controlling the balance between glutamate uptake and release, Cells 8 (2) (2019) 184.
[16] D. Klinger, K. Landfester, Stimuli-responsive microgels for the loading and release of functional compounds: fundamental concepts and applications, Polymer 53 (23) (2012) 5209–5231.
[17] C. Alvarez-Lorenzo, A. Concheiro, Smart drug delivery systems: from fundamentals to the clinic, Chem. Commun. 50 (2014) 7743–7765.
[18] M.N. Yasin, D. Svirskis, A. Seyfoddin, I.D. Rupenthal, Implants for drug delivery to the posterior segment of the eye: a focus on stimuli-responsive and tunable release systems, J. Contr. Release 196 (2014) 208–221.
[19] A.A. Moghanjoughi, D. Khoshnevis, A. Zarrabi, A concise review on smart polymers for controlled drug release, Drug Deliv. Translat. Res. 6 (2016) 333–340.
[20] C. Di Natale, V. Onesto, E. Lagreca, R. Vecchione, P.A. Netti, Tunable release of curcumin with an in silico-supported approach from mixtures of highly porous PLGA microparticles, Materials (Basel) 13 (8) (2020) 1807.
[21] I. Chernov, H. Greb, U. Janssen-Bienhold, J. Parisi, R. Weiler, E. von Hauff, Binding and potential-triggered release of L-glutamate with molecularly imprinted polypyrrole in neutral pH solutions, Sensor. Actuator. B Chem. 203 (2014) 327–332.
[22] N. Paul, M. Müller, A. Paul, E. Guenther, I. Lauermann, P. Müller-Buschbaum, M.C. Lux-Steiner, Molecularly imprinted conductive polymers for controlled trafficking of neurotransmitters at solid–liquid interfaces, Soft Matter 9 (2013) 1364–1371.
[23] B. Deore, Z. Chen, T. Nagaoka, Potential-induced enantioselective uptake of amino acid into molecularly imprinted overoxidized polypyrrole, Anal. Chem. 72 (17) (2000) 3989–3994.
[24] J. Tang, L. Zong, B. Mu, Y. Kang, A. Wang, Attapulgite/carbon composites as a recyclable adsorbent for antibiotics removal, Kor. J. Chem. Eng. 35 (8) (2018) 1650–1661.
[25] D.K.A. Zaini, N. Ngadi, M.A. Azman, K. Ahmad, Utilization of polyethylenimine (PEI) modified carbon black adsorbent derived from tire waste for the removal of aspirin, J. Pharm. Pharmacol. 79 (4) (2019) 222–227.
[26] M. Hasan, M.M. Rashid, M.M. Hossain, M.K. Al Mesfer, M. Arshad, M. Danish, M. Lee, A. El Jery, N. Kumar, Fabrication of polyaniline/activated carbon composite and its testing for methyl orange removal: optimization, equilibrium, isotherm and kinetic study, Polym. Test. 77 (2019) 105909.
[27] P.N. Diagboya, E.D. Dikio, Scavenging of aqueous toxic organic and inorganic cations using novel facile magneto-carbon black-clay composite adsorbent, J. Clean. Prod. 180 (2018) 71–80.
[28] M. Vomero, I. Dryg, T. Maxfield, W. Shain, S. Perlmutter, S. Kassegne, *In-Vivo* characterization of glassy carbon μ-electrodes and histological analysis of brain tissue after chronic implants, ECS Transact. 72 (1) (2016).
[29] M. Vomero, E. Castagnola, F. Ciarpella, E. Maggiolini, N. Goshi, E. Zucchini, S. Carli, L. Fadiga, S. Kassegne, D. Ricci, Highly stable glassy carbon interfaces for long-term neural stimulation and low-noise recording of brain activity, Sci. Rep. 7 (2017) 40332.
[30] B. Chen, B. Zhang, C. Chen, J. Hu, J. Qi, T. He, P. Tian, X. Zhang, G. Ni, M.M.-C. Cheng, Penetrating glassy carbon neural electrode arrays for brain–machine interfaces, Biomed. Microdevices 22 (3) (2020) 43.
[31] M. Vomero, A. Oliveira, D. Ashouri, M. Eickenscheidt, T. Stieglitz, Graphitic carbon electrodes on flexible substrate for neural applications entirely fabricated using infrared nanosecond laser technology, Sci. Rep. 8 (2018) 14749.
[32] S. Nimbalkar, E. Castagnola, A. Balasubramani, A. Scarpellini, S. Samejima, A. Khorasani, A. Boissenin, S. Thongpang, C. Moritz, S. Kassegne, Ultra-capacitive carbon neural probe allows simultaneous long-term electrical stimulations and high-resolution neurotransmitter detection, Sci. Rep. 8 (1) (2018) 6958.
[33] Y. Whulanza, D.S. Widyaratih, J. Istiyanto, G. Kiswanto, Realization and testing of lab-on-chip for human lung replication, ARPN J. Eng. Appl. Sci. 9 (11) (2014) 2064–2067.
[34] M.H. Nadhif, Y. Whulanza, J. Istiyanto, B.M. Bachtiar, Delivery of Amphotericin B to Candida albicans by using biomachined lab-on-a-chip, J. Biomimet. Biomater. Biomed. Eng. 30 (2017) 24–30.
[35] I.D. Sagita, Y. Whulanza, R. Dhelika, I. Nurhadi, Designing electrical stimulated bioreactors for nerve tissue engineering, AIP Conf. Proc. 1933 (2018), 040019.
[36] Y.B. Arafat, Y. Whulanza, Realizing textured electrode for electrochemical biosensor using homemade CNC desktop, AIP Conf. Proc. 2344 (1) (2021), 050019.
[37] D01 Committee Test Methods for Rating Adhesion by Tape Test; ASTM International.
[38] C.X. Du, L. Han, S.L. Dong, L.H. Li, Y. Wei, A novel procedure for fabricating flexible screen-printed electrodes with improved electrochemical performance, IOP Conf. Ser. Mater. Sci. Eng. 137 (1) (2016), 012060.
[39] H. Menon, R. Aiswarya, K.P. Surendran, Screen printable MWCNT inks for printed electronics, RSC Adv. 7 (2017) 44076–44081.
[40] K. Zheng, A. Scimemi, D.A. Rusakov, Receptor actions of synaptically released glutamate: the role of transporters on the scale from nanometers to microns, Biophys. J. 95 (2008) 4584–4596.
[41] J.V. Selkirk, L.M. Nottebaum, A.M. Vana, G.M. Verge, K.B. Mackay, T.H. Stiefel, G.S. Naeve, J.E. Pomeroy, R.E. Petroski, J. Moyer, J. Dunlop, A.C. Foster, Role of the GLT-1 subtype of glutamate transporter in glutamate homeostasis: the GLT-1-preferring inhibitor WAY-855 produces marginal neurotoxicity in the rat hippocampus, Eur. J. Neurosci. 21 (12) (2005) 3217–3228.
[42] M.A. Herman, C.E. Jahr, Extracellular glutamate concentration in hippocampal slice, J. Neurosci. 27 (36) (2007) 9736–9741.
[43] T. Yamashita, T. Kanda, K. Eguchi, T. Takahashi, Vesicular glutamate filling and AMPA receptor occupancy at the calyx of Held synapse of immature rats, J. Physiol. 587 (Pt 10) (2009) 2327–2339.
[44] N. Wisniewski, M. Reichert, Methods for reducing biosensor membrane biofouling, Colloids Surf. B Biointerfaces 18 (3-4) (2000) 197–219.
[45] J. Romanos, D. Benke, A.S. Saab, H.U. Zeilhofer, M. Santello, Differences in glutamate uptake between cortical regions impact neuronal NMDA receptor activation, Commun. Biol. 2 (1) (2019) 127.
[46] C.R. Rose, L. Felix, A. Zeug, D. Dietrich, A. Reiner, C. Henneberger, Astroglial glutamate signaling and uptake in the hippocampus, Front. Mol. Neurosci. 10 (2018) 451.

[47] N. Wisniewski, M. Reichert, Methods for reducing biosensor membrane biofouling, Colloids Surf. B Biointerfaces 18 (3-4) (2000) 197–219.
[48] S.H. Ku, M. Lee, C.B. Park, Carbon-based nanomaterials for tissue engineering, Adv. Healthcare Mater. 2 (2) (2013) 244–260.
[49] X. Navarro, T.B. Krueger, N. Lago, S. Micera, T. Stieglitz, P. Dario, A critical review of interfaces with the peripheral nervous system for the control of neuroprostheses and hybrid bionic systems, J. Peripher. Nerv. Syst. 10 (3) (2005) 229–258.
[50] S. Sharma, M. Madou, Micro and nano patterning of carbon electrodes for bioMEMS, Bioinspired, Biomimetic Nanobiomaterials 1 (4) (2012) 252–265.
[51] W. Zhang, S. Zhu, R. Luque, S. Han, L. Hu, G. Xu, Recent development of carbon electrode materials and their bioanalytical and environmental applications, Chem. Soc. Rev. 45 (3) (2016) 715–752.
[52] K. Scholten, E. Meng, Materials for microfabricated implantable devices: a review, Lab Chip 15 (22) (2015) 4256–4272.
[53] W. Zhang, S. Zhu, R. Luque, S. Han, L. Hu, G. Xu, Recent development of carbon electrode materials and their bioanalytical and environmental applications, Chem. Soc. Rev. 45 (3) (2016) 715–752.
[54] A.C. Patil, N.V. Thakor, Implantable neurotechnologies: a review of micro-and nanoelectrodes for neural recording, Med. Biol. Eng. Comput. 54 (1) (2016) 23–44.